Jet impingement onto a conical cavity with elevated wall temperature

B.S. Yilbas, S.Z. Shuja and M.O. Budair
ME Department, KFUPM, Dhahran, Saudi Arabia

Keywords *Jets, Turbulence, Flow, Heat transfer*

Abstract *Gas jet assisting process finds wide application in industry due to its ability to alter the heat transfer characteristics of the region subjected to jet assisted processing. In the present study, jet impingement onto a cavity with elevated wall temperature is considered. The flow and heat transfer equations are solved numerically using a control volume approach. Reynolds Stress Turbulence Model is employed to account for the turbulence. The simulations are repeated for four cavity depths and two gas jet velocities. It is found that the stagnation zone moves slightly further into the cavity with increasing cavity depth. The flow generated behind the stagnation zone in the cavity influences the heat transfer characteristics in this region, particularly for the cavities with relatively large depth.*

Nomenclature

H = enthalpy
K = thermal conductivity
k = turbulent kinetic energy
p = pressure
P = rate of production
R_{ij} = Reynolds stress
Re = Reynolds number
r = distance in the radial direction
t = time
T = temperature
u* = friction velocity
U = arbitrary velocity
$\forall$ = volume
x = distance in the axial direction
x_n = distance to the nearest wall
x_{max} = distance to the solid rear surface

Greek

α = thermal diffusivity
Γ = arbitrary diffusion coefficient
ε = energy dissipation
λ = turbulence intensity
μ = dynamic viscosity
ν = kinematic viscosity
ρ = density (function of temperature and pressure for gas)
σ = variable Prandtl number
Φ = viscous dissipation
ϕ = arbitrary variable
Π = energy transport due to pressure excluding strain interactions
Π^w = energy transport due to wall reflection
Λ = energy transport by diffusion

Subscript

amb = ambient
i, j = arbitrary direction
jet = gas jet at inlet
l = laminar
p = a typical node in the computational grid
t = turbulent
n, s, e, w, l, h = north, south, east, west, low or high node
w = wall

The authors acknowledge the support of King Fahd University of Petroleum and Minerals, Dhahran, Saudi Arabia for this work.

International Journal of Numerical Methods for Heat & Fluid Flow
Vol. 14 No. 8, 2004
pp. 1011-1028

0961-5539
DOI 10.1108/09615530410557423

1. Introduction

Gas jet assisted processing finds application in industry due to the achievements of enhanced heat transfer rates from the heat transferring surfaces. In most cases, assisting gas jet impinges onto the surface with high Reynolds numbers, in which case, the impinging jet is turbulent and the flow structure in the stagnation region is complex. This is particularly true when the jet impinges onto a cavity with its size being comparable to the jet size. In metal processing, such as laser machining, energy source generates a cavity while an assisting gas impinges onto the cavity either protecting the cavity surface from the high temperature oxidation reactions or enhancing the exothermic reactions. The prevention or the initiation of the exothermic reaction in the cavity depends on the type of assisting gas employed. The use of inert gas such as argon or helium prevents the exothermic reaction while use of oxygen initiates the reaction. Beside the oxidation reaction, assisting gas has influence on the heat transfer characteristics of the cavity surface. Moreover, the cavity surface stays almost at the melting temperature of the substrate material during the laser processing. The thermodynamic pressure build in the surface vicinity of the cavity wall (due to high cavity wall temperature) influences the flow and heat transfer characteristics in the cavity. Consequently, investigation of the jet impingement onto cavities and heat transfer rates from the cavity surfaces is fruitful for industrial applications.

Considerable research studies were carried out to explore the jet impingement situations. Impinging jet studies for turbulence model assessment were carried out by Craft *et al.* (1993). They indicated that the two-equation model over predicted the turbulence kinetic energy in the stagnation region and Reynolds Stress Turbulence Model predictions were in acceptable agreement with the experimental results. The Reynolds stress model assessment using round jet experimental data was presented by Lasher and Taulbee (1994). They showed that predictions using the linear models were generally as good as those obtained from non-linear models; in which case, non-linear models might not be necessary for engineering accuracy for the impinging jet situations. Stagnation turbulent flows were investigated by Strahle *et al.* (1987). They demonstrated that at high Reynolds numbers, an effect of the stagnation process in the nonviscous zone outside the boundary layer predicted an excessive effect of body size on the results, although the agreement was still satisfactory. The axisymmetric and two-dimensional impinging turbulent jets were studied by Dianat *et al.* (1996). The $k - \varepsilon$ turbulence model and a version of a second-moment closure, modified to include the effect of pressure reflections from a surface, were used in the analysis. They showed that results obtained from the eddy-viscosity-based approach did not, in general, accurately reproduced the experimental observations.

The heat transfer characteristics of a surface due to impinging jet were investigated extensively to explore the physical processes involved. A comprehensive review on heat transfer under impinging jets was carried out by Polat *et al.* (1989). They indicated that prediction of flow, heat, and mass transfer under a single, semi-confined turbulent jet might be employed as a good test for new turbulence models. A review of heat transfer data for single circular jet impingement was presented by Jambunathan *et al.* (1992). They suggested that the Nusselt number was independent of nozzle-to-plate spacing upto a value of 12 nozzle diameters at radii greater than nozzle diameters from the stagnation point. Heat transfer measurements from a surface with uniform heat flux and an impinging jet were studied by Baughn and Shimizu (1989). They showed

that the maximum stagnation point heat transfer occurred for ratio of wall to nozzle spacing to nozzle diameter (z/D) of approximately 6. The effect of ambient air entrainment into a heated impinging jet on the heat transfer from a flat plate surface was investigated by Baughn *et al.* (n.d.). They indicated that it was possible to use heat transfer data for the heated jet, if the effectiveness was known and the local heat transfer coefficient was defined in terms of the adiabatic wall temperature. The local heat transfer coefficient distribution on a square heat source due to a normally impinging axisymmetric, confined, and submerged liquid jet was studied by Morris *et al.* (1996). They indicated that the predicted heat transfer coefficients were in good agreement with the experimental results. Turbulent planar jet impinging onto a slot was studied by Tchavdarov (1997) using Chorin's random vortex method. He showed that the impinging vortex rebounds from the solid wall and a secondary vortex was ejected from the viscous layer. The characteristics of turbulent submerged axisymmetric incompressible jets impinging on a flat plate and flowing into axisymmetric cavity were studied by Amano and Brandt (1984). They showed that the velocity profile and the turbulence intensity at the nozzle exit affected the magnitude of the maximum skin friction on the wall.

In the light of the above arguments, the present study is carried out to examine the flow and heat transfer characteristics of jet impingement onto a conical cavity with elevated wall temperature. The cavity wall temperature enables to examine the influence of the thermodynamic pressure on the flow and heat transfer characteristics. In the analysis, impinging gas is assumed to be inert, therefore, high temperature exothermic reaction is neglected. The numerical scheme using a control volume approach is introduced to solve the governing equations of flow and heat transfer. Reynolds stress turbulence model is employed to account for the turbulence.

2. Mathematical modelling

In the process industry, the impinging jet conditions are mainly steady; consequently, a steady flow conditions are considered in the analysis. The compressibility effect and variable properties are accommodated as well as temperature dependent thermal conductivity and specific heat are considered for the solid substance. The jet impinging onto the conical cavity with constant wall temperature (1,500 K) situation is simulated for two jet velocities and four cavity depths. The geometric arrangement of the jet and the cavity in the solid substrate are shown in Figure 1 while the cavity depths are given in Table I.

2.1 Flow equations

The governing flow and energy equations for the axisymmetric impinging jet can be written in the Cartesian tensor notation as:

The continuity equation is:

$$\frac{\partial}{\partial x_i}(\rho U_i) = 0 \tag{1}$$

The momentum equation is:

$$\frac{\partial}{\partial x_i}(\rho U_i U_j) = -\frac{\partial p}{\partial x_j} + \frac{\partial}{\partial x_i}\left[\mu\left(\frac{\partial U_i}{\partial x_j} + \frac{\partial U_j}{\partial x_i}\right) - \rho R_{ij}\right] \tag{2}$$

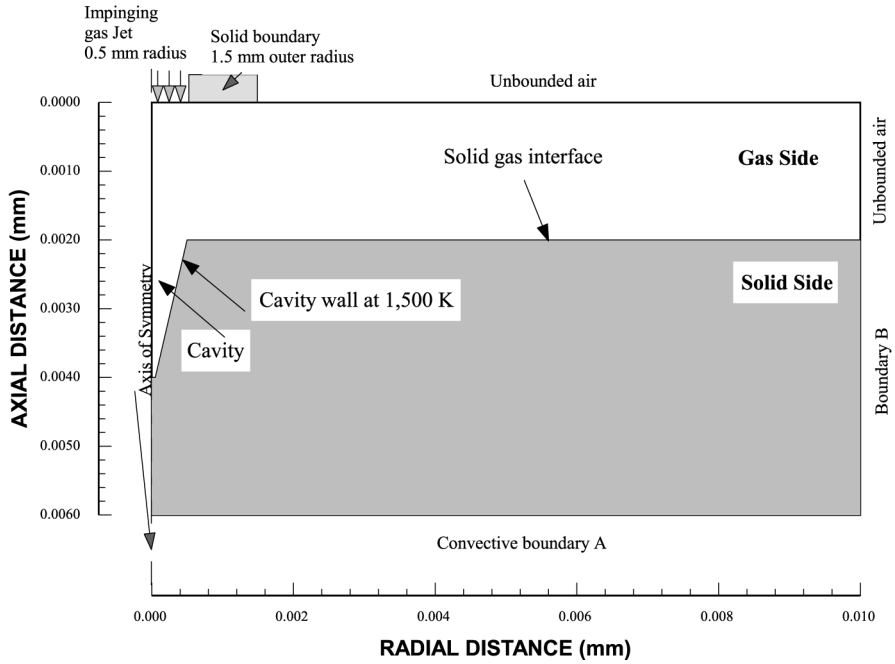

Figure 1.
The solution domain with arrangement of the boundaries

Cases	Cavity depths (mm)
1	0.2
2	0.5
3	1
4	2

Table I.
Cavity depths for different cases

The energy equation is:

$$\frac{\partial}{\partial x_i}(\rho U_i H) = \frac{\partial}{\partial x_i}\left[\frac{\mu}{\sigma}\frac{\partial H}{\partial x_i} - \rho R_{ih}\right] \tag{3}$$

when modelling the Reynolds stresses and turbulence properties following steps are considered.

2.1.1 Reynolds stresses (R_{ij}). The RSTM is based on the second-moment closure (Launder and Rodi, 1983). The transport equation of the Reynolds stress (R_{ij}) is:

$$\frac{\partial}{\partial x_m}(U_m R_{ij}) = P_{ij} + \Lambda_{ij} - \varepsilon_{ij} + \Pi_{ij} + \Pi_{ij}^{w} \tag{4}$$

where P, Λ, ε, Π and Π^{w} are the rate of production, transport by diffusion, rate of dissipation, transport due to turbulent pressure excluding strain interactions and transport due to wall reflection, respectively. Equation (4) consists of six partial differential equations; one for the transport of each of the six independent Reynolds

stresses. The production term (P_{ij}), diffusion (Λ_{ij}), dissipation (ε_{ij}), transport due to turbulent pressure (Π_{ij}) and the modelling of the wall reflection (Π_{ij}^{w}) are refereed to Launder and Rodi (1983).

2.2 Heat conduction equation

The heat conduction in a stationary solid medium can be formulated using the Fourier heating model. Therefore, the equation governing the heat conduction yields a modified form of equation (3), i.e.

$$K\,\frac{\partial}{\partial x_i}\left[\frac{\partial T}{\partial x_i}\right] = 0 \tag{5}$$

where K is the thermal conductivity of solid.

2.3 Flow boundary conditions

Four boundary conditions are considered in accordance with the geometric arrangement of the problem as shown in Figure (1); these are:

Solid wall. No slip condition is assumed at the solid wall and the boundary condition for the velocity at the solid wall is therefore:

$$U_i = 0$$

Generalized wall functions for normal and shear turbulent stresses for the RSTM models. When the flow is very near the wall it undergoes a rapid change in direction, the wall-functions approach is not successful in reproducing the details of the flow. Consequently, the turbulent stresses and fluxes at the near wall grid points are calculated directly from their transport equations. In this case, the near-wall region lying between the wall and the near-wall computational node at x_p can be represented by two layers: the fully viscous sublayer, defined by $\mathrm{Re}_v = x_v\sqrt{k_v}/\nu \cong 20$, and a fully-turbulent layer. The wall shear stress near the wall is employed, i.e. $\overline{vw}|_{z_v} = \tau_w/\rho$, which serves as the boundary condition for the $\overline{vw}$ transport equation.

In relation to normal stresses, the turbulence energy must decrease quadratically towards a value of zero at the wall (Benocci, 1991), therefore, a zero-gradient condition for the normal stresses is physically realistic. This situation is insufficient to ensure an accurate numerical representation of near-wall effects. An improved approach for internal cells is needed in respect of evaluating volume-integrated production and dissipation of normal stresses (these are normally evaluated at cell centres, using linear interpolation, and then multiplied by the cell volume). Considering $\overline{v^2}$ as an example, the volume-integrated production of $\overline{v^2}$ between the wall and the P-node may be approximated by Hogg and Leschziner (1989), i.e.:

$$\int_{\Delta r}\int_{0}^{z_p} P_{22}\,\mathrm{d}\forall \cong \int_{\Delta r}\int_{z_v}^{z_p} -2\overline{vw}\,\frac{\partial V}{\partial x}\,\mathrm{d}\forall = 2\tau_w\left(\frac{V_p - V_v}{x_p - x_v}\right)x_p\Delta r \tag{6}$$

where V_p and V_v follow from the log-law. No contribution arises from the viscous sublayer since $\overline{vw} = 0$ in this layer. An analogous integration of the dissipation rate with the assumptions,

$$\varepsilon = \frac{2\nu k_v}{x_v^2} \qquad 0 \le x \le x_v$$

$$\varepsilon = \frac{C_\mu^{3/4} k_p^{3/2}}{\kappa x_v} \qquad x_v \le x < x_p$$

leads to

$$\int_{\Delta r} \int_0^{x_p} \varepsilon \, \mathrm{d}\forall \cong \left[\frac{2\nu k_p}{x_v} + \frac{C_\mu^{3/4} k_p^{3/2}}{\kappa} \ln\left(\frac{x_p}{x_v}\right) \right] \Delta r \tag{7}$$

an analogous treatment is applied to $\overline{v^2}$, while the production of $\overline{w^2}$ in the viscous and turbulent near wall layers region is zero (Versteeg and Malalasekera, 1995).

The values resulting from equations (6) and (7) are added, respectively, to the volume-integrated generation and dissipation computed for the upper half of the near-wall volume.

It should be noted that for the wall-law approach, the near-wall dissipation (ε_p) is not determined from its differential equation applied to the near-wall cell surrounding the node. Instead, and in accordance with the log law, this value is obtained via the length scale from

$$\varepsilon_p = \frac{C_\mu^{3/4} k_p^{3/2}}{\kappa z_p},$$

which serves as the boundary conditions for inner cells.

Inlet conditions. The boundary conditions for temperature and velocity need to be introduced:

$$T = \text{specified } (300\,\text{K}) \text{ and } U = \text{specified } (50\,\text{m/s} \text{ and } 100\,\text{m/s})$$

The values of k and ε are not known at the inlet, but can be determined from turbulent kinetic energy i.e.:

$$k = \lambda \bar{u}^2 \tag{8}$$

where $\bar{u}$ is the average inlet velocity and λ is a percentage.

The dissipation is calculated from:

$$\varepsilon = C_\mu \frac{k^{\frac{3}{2}}}{aD},$$

where D is the diameter. The values $\lambda = 0.03$ and $a = 0.005$ are commonly used and may vary slightly in the literature (Bradshaw *et al.*, 1981).

Outlet. The flow is considered to be extended over a long domain; therefore, the boundary condition (unbounded boundaries – Figure (1)) for any variable ϕ is:

$$\frac{\partial \phi}{\partial x_i} = 0 \tag{9}$$

where x_i is the normal direction at outlet.

Symmetry axis. At the symmetry axis, the radial derivative of the variables is set to zero, i.e.:

$$\frac{\partial \phi}{\partial r} = 0 \tag{10}$$

except

$$V = \overline{vw} = \overline{vh} = \overline{wh} = 0$$

2.3.1 Solid side. Constant temperature boundary. Two constant temperature boundaries are considered. First one is in the radial direction far away from the symmetry axis constant temperature $T = T_{\text{amb}}$ (300 K) is defined (boundary A in Figure (1)). It should be noted that the constant temperature boundary condition is set at different locations in the radial directions at boundary A and no significant effect of $T =$ constant was observed on the temperature and flow field in the stagnation region. Therefore, this boundary condition is set for radial distance 0.010 m from the symmetry axis. The second constant temperature boundary is set at the cavity wall (as shown in Figure (1)) $T =$ constant (1,500 K).

2.3.2 Solid fluid interface. The coupling of conduction within the solid and convection within the fluid, termed conjugation, is required for the present analysis at the solid fluid interface. The appropriate boundary conditions are continuity of heat flux and temperature and are termed boundary conditions of the fourth kind. i.e.:

$$T_{w_{\text{solid}}} = T_{w_{\text{gas}}}$$

$$K_{w_{\text{solid}}} \frac{\partial T_{w_{\text{solid}}}}{\partial x} = K_{w_{\text{gas}}} \frac{\partial T_{w_{\text{gas}}}}{\partial x}$$

No radiation losses from the solid surface is assumed.

2.4 Gas and solid properties

The equation of state is used for air and constant properties are employed for steel. The properties employed are given in Table II. The properties of the solid is assumed constant in the analysis.

2.5 Nusselt number ratios

The Nusselt number ratio is introduced to observe the relative magnitude of the Nusselt numbers corresponding to 50 and 100 m/s jet velocities.

Therefore, the Nusselt number ratio is:

$$\frac{(\text{Nu})_{V_j} = 50\,\text{m/s}}{(\text{Nu})_{V_j} = 100\,\text{m/s}}$$

Property		Gas (Air)	Solid (Steel)
Density	ρ (kg/m^3)	p/RT	8,030
Thermal conductivity	K (W/mK)	0.0242	16.27
Specific heat capacity	c_p (J/kg K)	1006.43	502.48
Viscosity	ν (kg/m s)	1.7894×10^{-5}	

Table II. Properties used in the simulation

3. Numerical method and simulation

A control volume approach is employed when discretizing the governing equations. The discretization procedure is given in Versteeg and Malalasekera (1995). The problem of determining the pressure and satisfying continuity may be overcome by adjusting the pressure field so as to satisfy continuity. A staggered grid arrangement is used in which the velocities are stored at a location midway between the grid points, i.e. on the control volume faces. All other variables including pressure are calculated at the grid points. This arrangement gives a convenient way of handling the pressure linkages through the continuity equation and is known as Semi-Implicit Method for Pressure-Linked Equations (SIMPLE) algorithm. The details of this algorithm is given in Patankar (1980).

The computer program used for the present simulation can handle a non-uniform grid spacing. In each direction fine grid spacing near the gas jet impinging point and the hole is allocated while gradually increased spacing for locations away from the hole is considered. Elsewhere the grid spacing is adjusted to maintain a constant ratio of any of the two adjacent spacings. The grid generated in the present study is shown in Figure (1). The number of grid planes used normal to the r and x directions are 90 and 70, respectively, thus making a total of 6,300 grid points. The grid independence tests were conducted and it was observed that for 90×110 grid points, the predictions were in excellent agreement with the results of 90×70 grid points, i.e. the difference in predictions is less than 0.1 per cent.

Six variables are computed at all grid points; these are: the two velocity components, the local pressure, the two turbulence quantities and the temperature.

4. Results and discussions

Jet impingement onto a conical cavity is investigated. The cavity wall is set to the elevated temperature. This enables us to examine the influence of the thermodynamic pressure on the flow and heat transfer characteristics. A numerical solution employing a control volume approach is introduced when solving the governing equations of flow and heat transfer. The simulations are repeated for four cavity depths and two assisting gas jet velocities.

Figure 2 shows the velocity vectors in the region of the cavity for different non-dimensional cavity depths and 100 m/s assisting gas jet velocity. It should be noted that the cavity depths are non-dimensionalized by the ratio of cavity depth to cavity diameter. When the cavity depth is zero, the flow becomes a stagnation point flow over a flat plate. As the depth increases, the impinging jet penetrates into the cavity and it streamlines in the radial direction developing the radial flow in the cavity exit. In the region close to the cavity bottom, flow becomes almost stagnant. As the cavity depth increases further, the depth of penetration of the impinging jet into the cavity increases and stagnation region moves further into the cavity. Moreover, due to elevated cavity wall temperature a thermal boundary layer is developed in the vicinity of the cavity wall. This results in thermodynamically high pressure region close to the wall, which in turn suppresses slightly the depth of penetration of the impinging jet into the cavity. In the case of large cavity depth ($L^* = 2$, where $L^* = L/D$ and L and D are the cavity depth and jet diameter, respectively), the flow in the cavity particularly in the region of the symmetry axis attains low velocities. Moreover, behind the stagnation region in the cavity, a flow is developed and the flow in the cavity due to

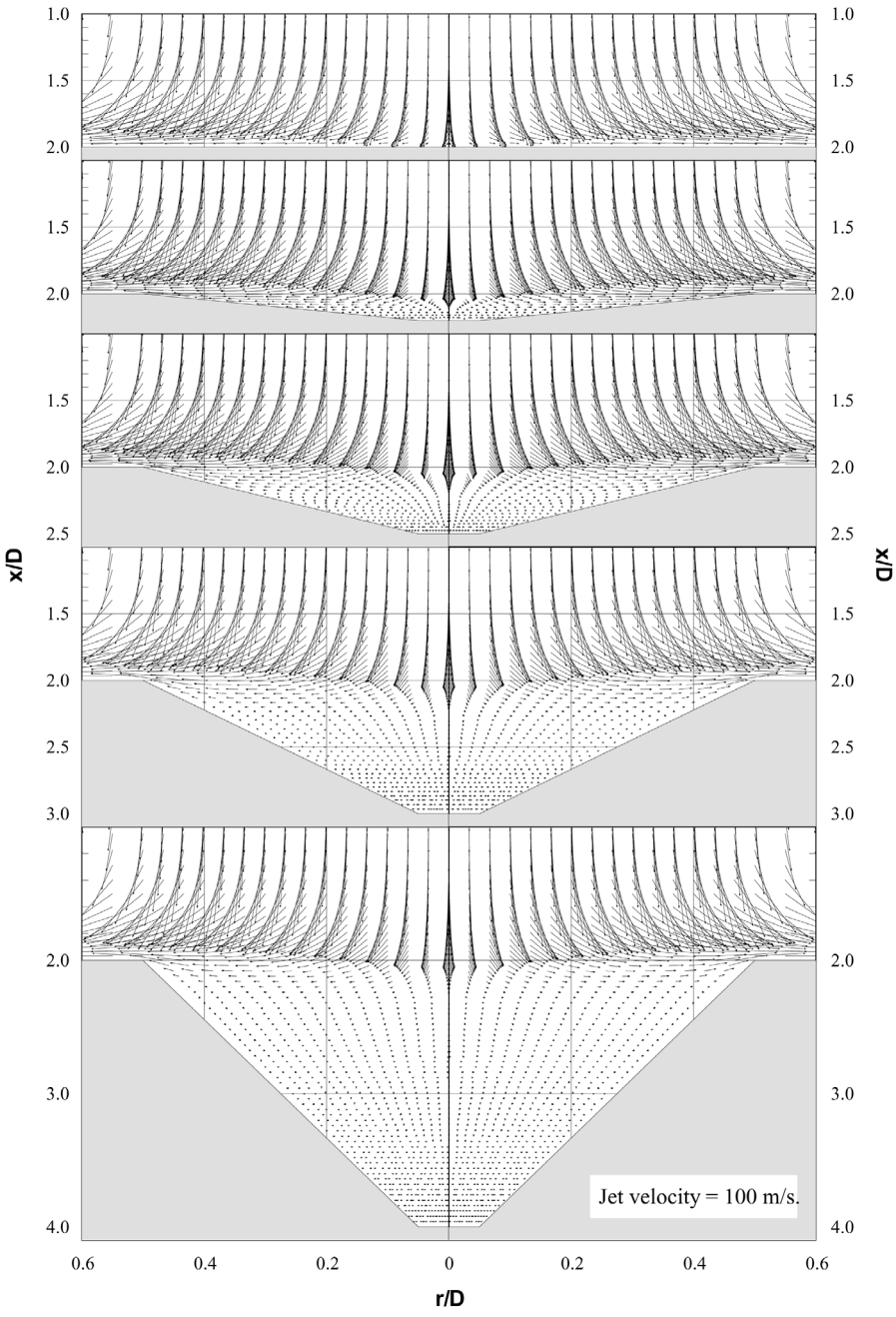

Figure 2.
Velocity vectors in and around the conical cavity

impinging jet opposes the thermally developed flow due to high wall temperature. Consequently, the hot gas in the surface region of the cavity-end remains almost stagnant.

Figure 3(a) shows the dimensionless velocity magnitude (V/V_j) along the symmetry axis (x/D and $r/D = 0$) is shown for two different non-dimensional cavity depths. Velocity magnitude reduces along the symmetry axis. The region where the velocity magnitude approaches zero indicates the stagnation region in the cavity. The influence

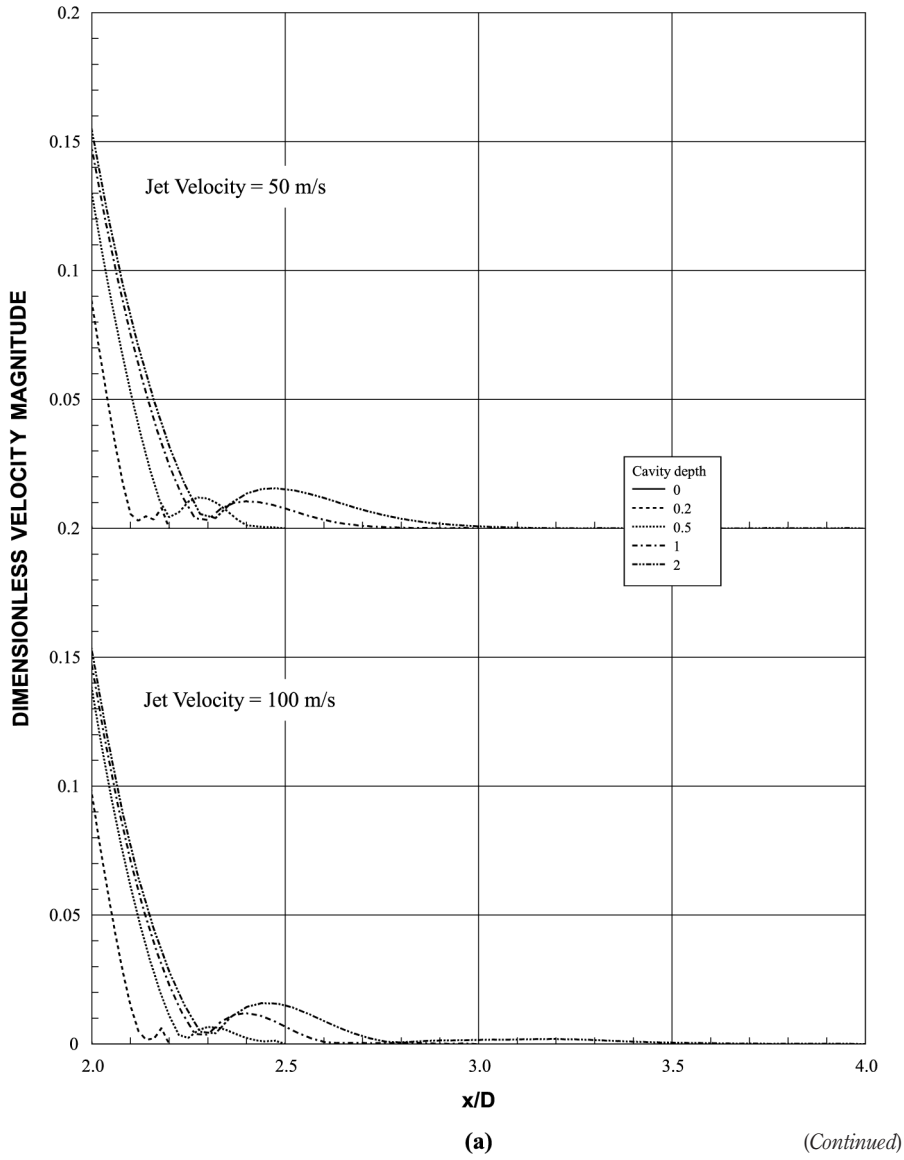

(*Continued*)

Figure 3.
(a) Velocity magnitude along the symmetry axis in the cavity; and
(b) Dimensionless velocity magnitude along the symmetry axis for solid wall temperature 300 and 1,500 K.

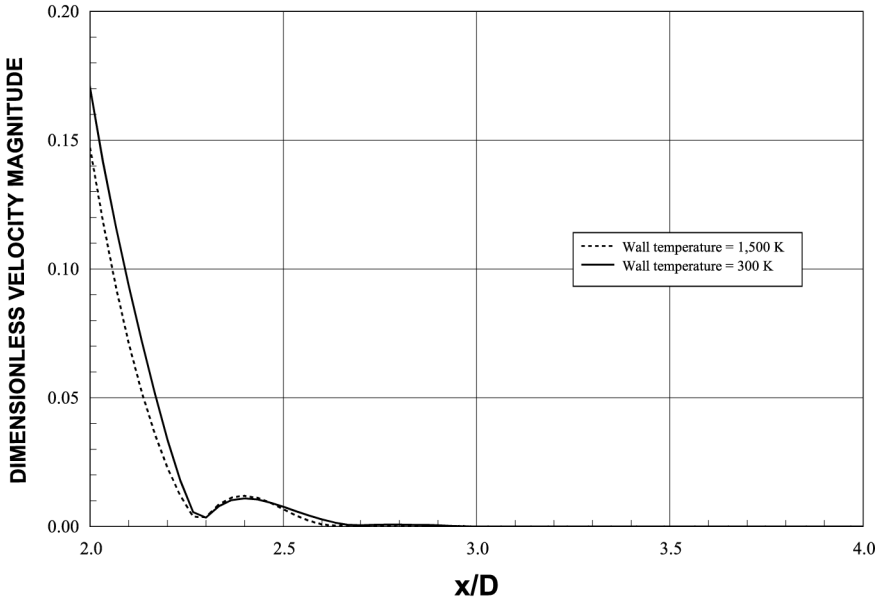

(b) The cavity depth is 1 mm and gas jet velocity is 100 m/s

Figure 3.

of high thermodynamic pressure on the flow in the cavity behind the stagnation region is not considerable, since the velocity magnitude resulted from elevated and room temperature cavity wall cases are similar. This can be seen from Figure 3(b), in which velocity magnitude is shown for the cavity depth of $L^* = 1$ and two cavity wall temperatures. It is evident that the high wall temperature reduces the velocity magnitude along the symmetry axis in the cavity provided that the location of stagnation region does not change.

Figure 4(a) shows pressure coefficient along the symmetry axis in the cavity for different non-dimensional cavity depths and two jet velocities. Pressure coefficient increases along the symmetry axis towards the cavity-end. This is more pronounced as the cavity depth increases. In this case, impinging jet penetrating the cavity has high velocity magnitude (Figure 3) as the cavity depth increases. This in turn reduces the local pressure rise along the symmetry axis; consequently, pressure coefficient reduces with increasing cavity depth. The influence of cavity wall temperature on pressure coefficient can be seen in Figure 4(b), in which pressure coefficient is shown for two cavity wall temperatures and cavity depth of $L^* = 1$. Pressure coefficient attain slightly lower values for the cavity with elevated wall temperature. The influence of gas jet velocity on pressure coefficient is considerable, in which case, the magnitude and behavior of pressure coefficient curves change, i.e. high gas jet velocity results in high pressure rise in the cavity.

Figure 5 shows the dimensionless temperature profiles along the symmetry axis inside the cavity for different non-dimensional cavity depths and two jet velocities. Temperature profiles rises sharply along the symmetry axis to reach the cavity wall temperature for cavity depth ≤ 0.5 ($L^* \leq 0.5$). As the cavity depth increases,

temperature rise becomes gradual behind the stagnation region. The gradual rise of temperature is because of the cavity flow generated in this region. In this case, the flow generated behind the stagnation region is heated by the high temperature cavity wall. Since the flow is not totally stagnant in this region, temperature of the fluid rises gradually as the distance increases from the stagnation region towards the cavity-end.

Figure 6 shows the Nusselt number variation in the radial direction. It should be noted that $r/D = 0$ represents the symmetry axis while $r/D = 1$ corresponds to the

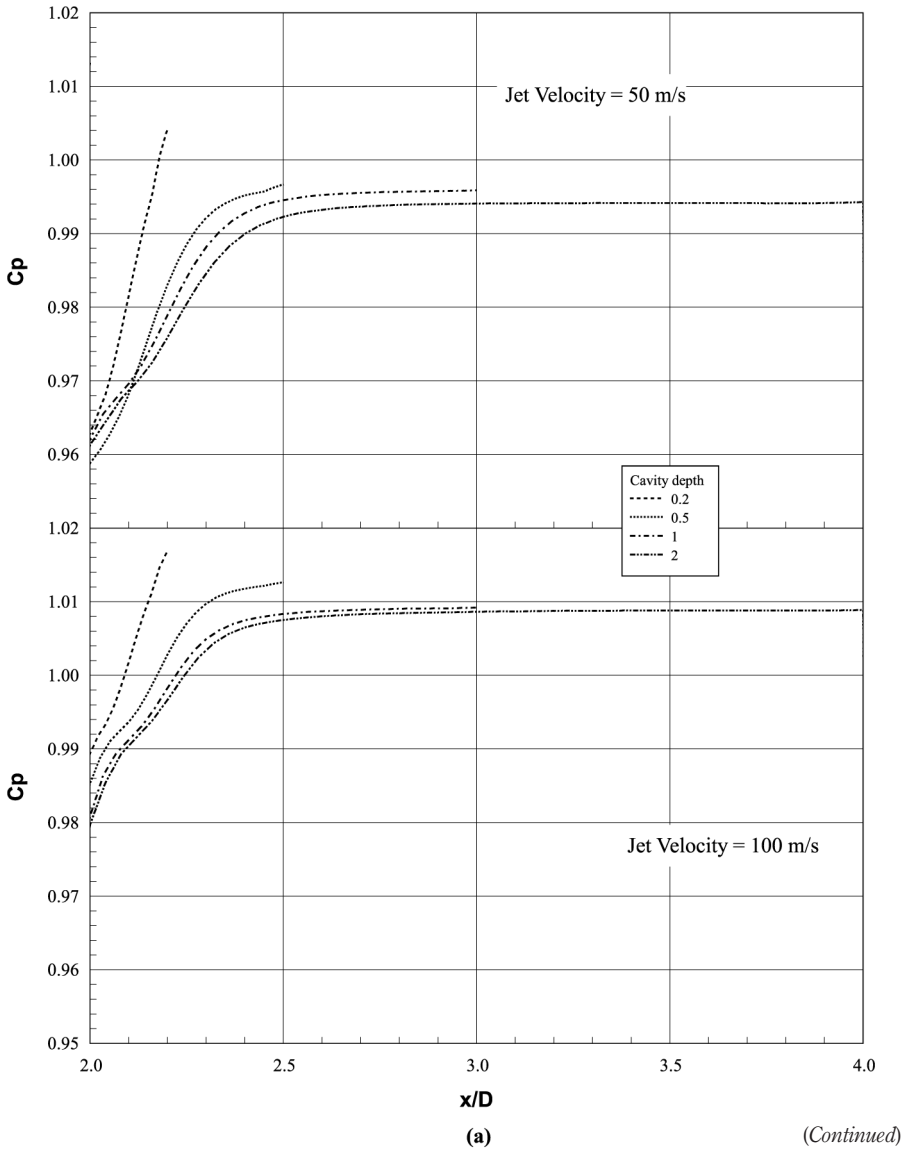

Figure 4.
(a) Pressure coefficient (*Cp*) profiles along the symmetry axis in the cavity; and (b) pressure coefficient (*Cp*) profiles along the symmetry axis for solid wall temperature 300 and 1,500 K

(*Continued*)

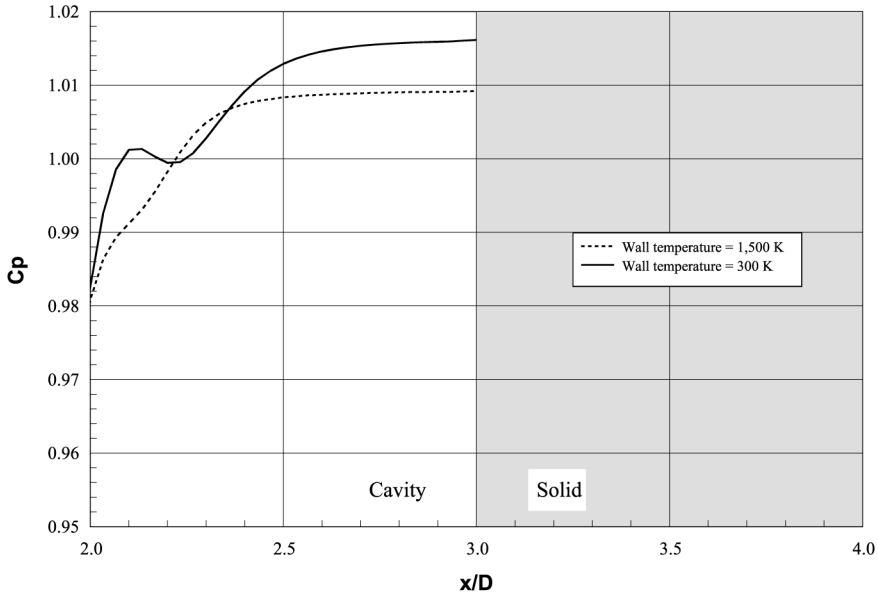

(b) The cavity depth is 1 mm and gas jet velocity is 100 m/s

Figure 4.

cavity exit in the radial direction. The Nusselt number attains considerably low values at the cavity-end. This is because of the development of almost stagnation zone in this region. As the distance increases in the radial direction, Nusselt number increases sharply. This is more pronounced for deep cavities. The influence of the stagnation region formed in the cavity on the Nusselt number is not clearly observed from the curves due to logarithmic plot. Moreover, the Nusselt number ratio (the ratio of the Nusselt number corresponding to 50 m/s jet velocity to its counterpart obtained for 100 m/s jet velocity) is shown in Figure 7. The Nusselt number ratio is less than one in the cavity indicating that the high gas jet velocity improves significantly the Nusselt number in the cavity. Moreover, the Nusselt number ratio varies considerably in the region close to the cavity exit. This is because of complex flow structure due to mixing of the flow exiting the cavity and the impinging jet in this region. The influence of the flow developed behind the stagnation region in the cavity on the Nusselt number ratio is evident. In this case, the Nusselt number ratio attains relatively higher values in this region.

Figure 8(a) shows the skin friction coefficient (C_f) in the cavity. C_f reduces considerably as the cavity depth increases. This is because of the slow flow regime developed in the cavity, which is particularly true in the region close to the symmetry axis. In order to examine the influence of cavity wall temperature on C_f, (Figure 8(b)) it can be observed that C_f is not significant.

5. Conclusions

Jet impingement onto a conical cavity with elevated wall temperature is considered. A numerical scheme using a control volume approach is employed to solve governing equations of flow and heat transfer. The Reynolds stress turbulence model is

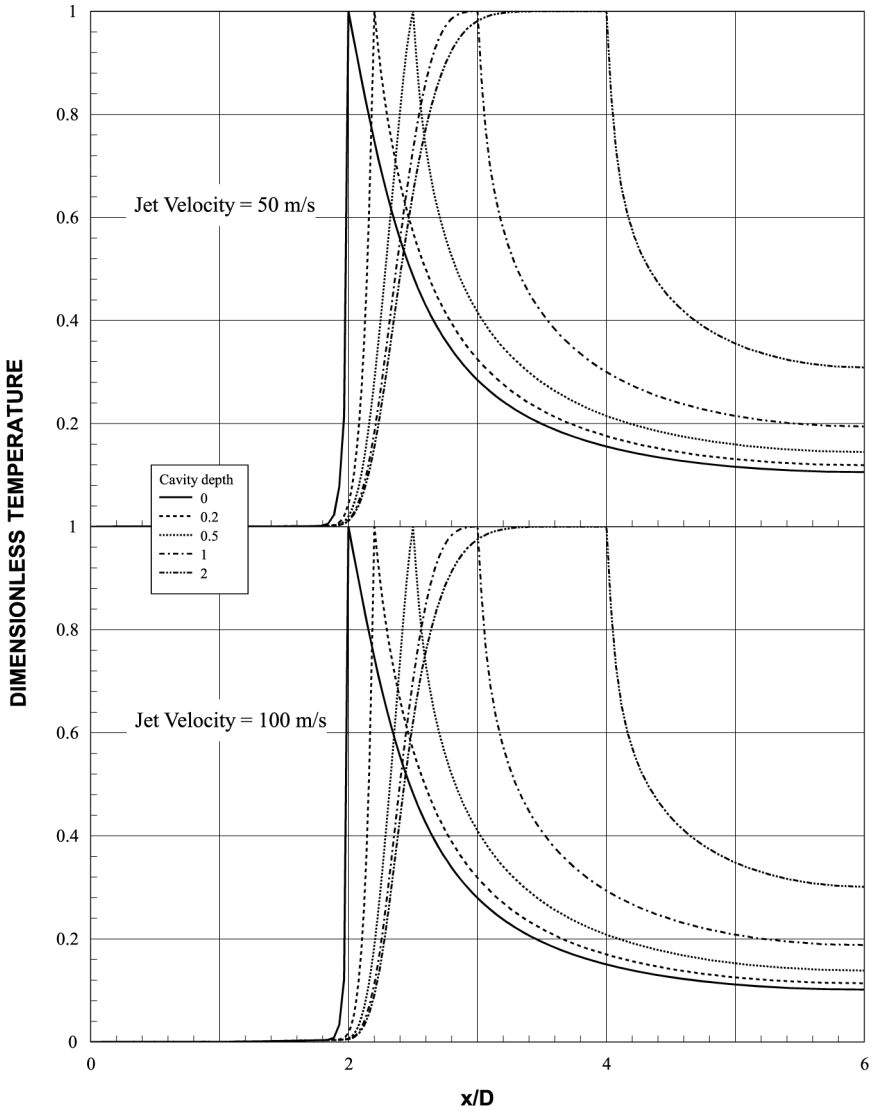

Figure 5.
Dimensionless temperature profiles along the symmetry axis in the gas and solid sides

accommodated to account for the turbulence. The simulations were repeated for four cavity depths and two impinging jet velocities. It is found that the stagnation region moves into the cavity as the depth increases. The influence of cavity depth on the flow field, which is generated behind the stagnation region in the cavity is considerable. The specific conclusions derived from the present work can be listed as follows.

(1) Velocity magnitude reduces sharply for shallow cavities and the flow behind the stagnation region is developed in the cavity. The influence of the cavity wall

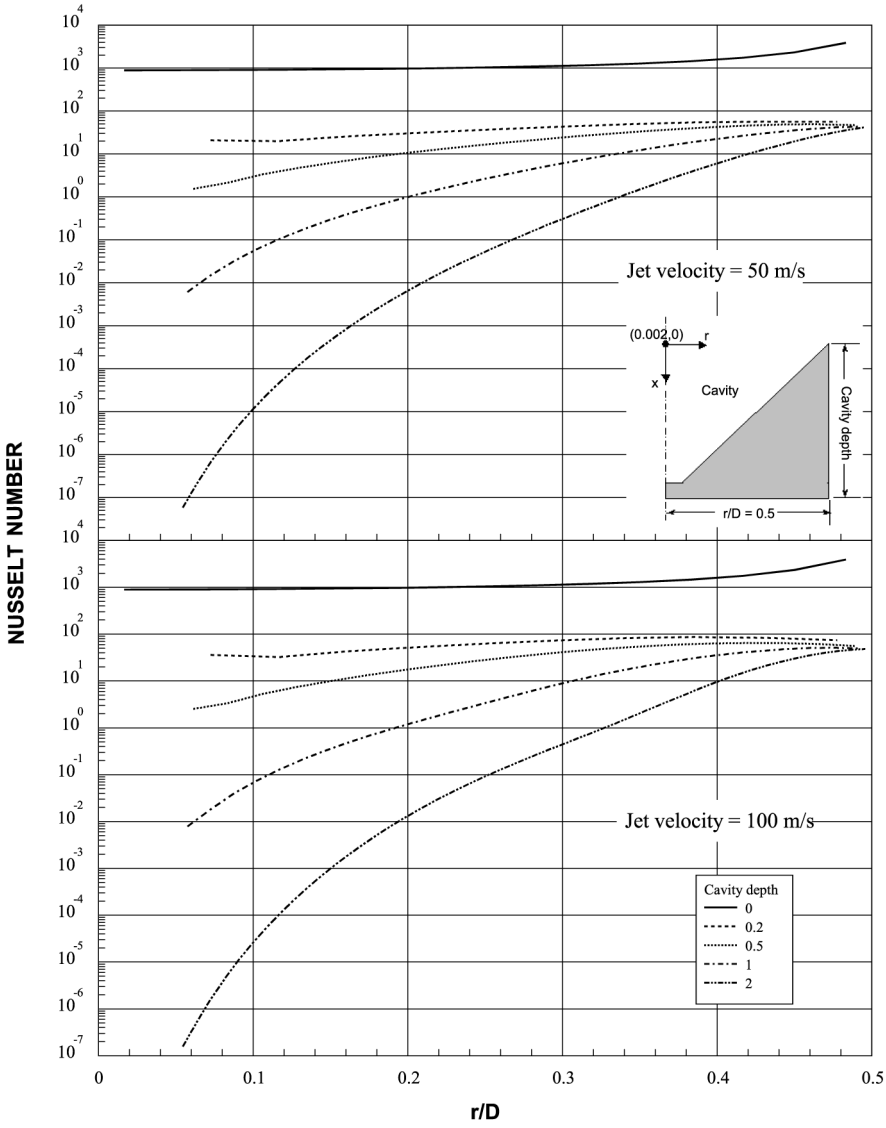

Figure 6.
The Nusselt number variation along the radial direction in the cavity

temperature on the flow behind the stagnation region is not considerable along the symmetry axis.

(2) Temperature profiles decays gradually in the cavity for deep cavities. This is because of the development of the flow behind the stagnation region in the cavity.

(3) The influence of the cavity wall temperature on the pressure coefficient along the symmetry axis is found to be significant in the cavity entry region.

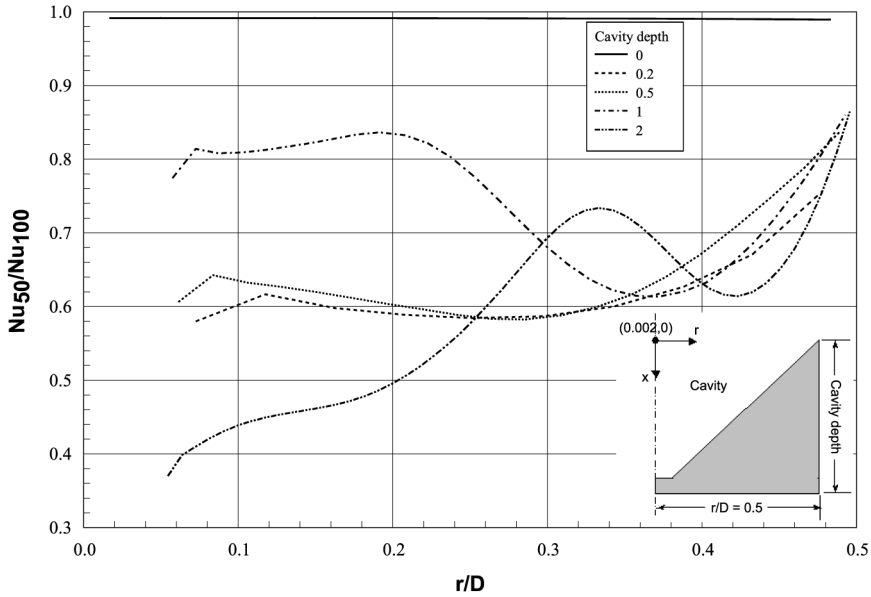

Figure 7.
The Nusselt ratio variation along the radial direction in the cavity

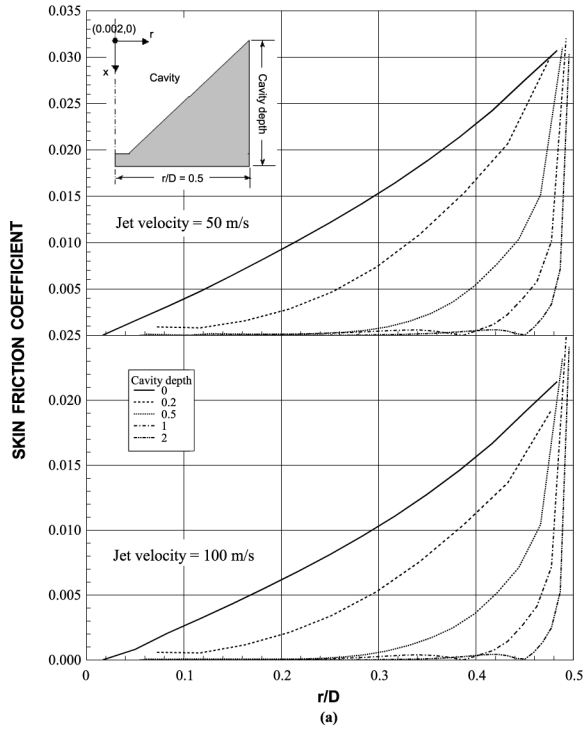

Figure 8.
(a) The skin friction coefficient variation along the radial direction in the cavity; and (b) the skin friction coefficient variation along the radial direction in the cavity

(*Continued*)

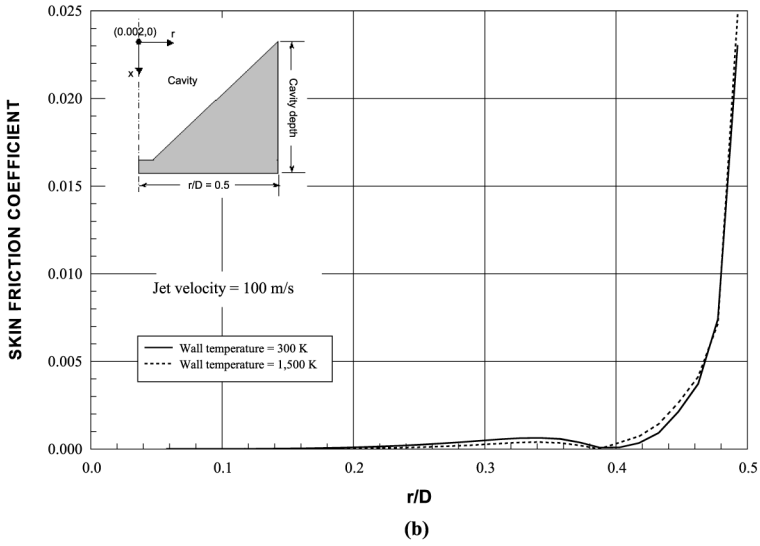

Figure 8.

Moreover, the pressure coefficient along the symmetry axis in the cavity reduces gradually with increasing cavity depth and the behavior of pressure coefficient curves differs for two gas jet velocities.

(4) The Nusselt number increases gradually in the radial direction towards the cavity exit for deep cavities. The influence of the flow behind the stagnation region on the Nusselt number is more pronounced for high jet velocity (100 m/s).

(5) The skin friction coefficient attains low values for deep cavities and the influence of cavity wall temperature on the skin friction is found to be insignificant.

References

Amano, R.S. and Brandt, H. (1984), "Numerical study of turbulent axisymmetric jets impinging on a flat plate and flowing into an axisymmetric cavity", *ASME, J. Fluids Engineering*, Vol. 106, pp. 410-7.

Baughn, J.W. and Shimizu, S. (1989), "Heat transfer measurements from a surface with uniform heat flux and an impinging jet", *ASME Journal of Heat Transfer*, Vol. 111, pp. 1096-8.

Baughn, J.W., Hechanova, A.E. and Yan, X. (n.d.), "An experimental study of entrainment effects on the heat transfer from a flat surface to a heated circular impinging jet", *ASME J. Heat Transfer*, Vol. 113, pp. 1023-5.

Benocci, C. (1991), *Introduction to the Modeling of Turbulence*, Von Karman Institute for Fluid Dynamics, pp. 1991-2002.

Bradshaw, P., Cebeci, T. and Whitelaw, J.H. (1981), *Engineering Calculation Methods for Turbulent Flow*, Chapter 3, Academic Press, New York, NY, p. 51.

Craft, T.J., Graham, L.J.W. and Launder, B.E. (1993), "Impinging jet studies for turbulence model assessment-II an examination of the performance of four turbulence models", *International Journal of Heat and Mass Transfer*, Vol. 36 No. 10, pp. 2685-97.

Dianat, M., Fairweather, M. and Jones, W.P. (1996), "Predictions of axisymmetric and two-dimensional impinging turbulent jets", *Int. J. Heat and Fluid Flow*, Vol. 17, pp. 530-8.

Hogg, S. and Leschziner, M.A. (1989), "Second-moment-closure calculation of strongly swirling confined flow with large density gradients", *International Journal of Heat and Fluid Flow*, Vol. 10 No. 1, pp. 16-27.

Jambunathan, K., Lai, E., Moss, M.A. and Button, B.L. (1992), "A review of heat transfer data for single circular jet impingement", *International Journal of Heat and Fluid Flow*, Vol. 13, pp. 106-15.

Lasher, W.C. and Taulbee, D.B. (1994), "Reynolds stress model assessment using round jet experimental data", *International Journal of heat and Fluid Flow*, Vol. 15 No. 5, pp. 357-63.

Launder, B.E. and Rodi, W. (1983), "The turbulent wall jet – measurement and modeling", *Annual Review of Fluid Mechanics*, Vol. 15, pp. 429-33.

Morris, G.K., Gaimella, S.V. and Amano, R.S. (1996), "Prediction of jet impingement heat transfer using a hybrid wall treatment with different turbulent Prandtl number functions", *Journal of Heat Transfer*, Vol. 118, pp. 562-9.

Patankar, S.V. (1980), *Numerical Heat Transfer*, McGraw-Hill, New York, NY.

Polat, S., Huang, B., Mujumdar, S. and Douglas, W.J.M. (1989), "Numerical flow and heat transfer under impinging jets: a review", *Volume 2 of Annual Review of Numerical Fluid Mechanics and Heat Transfer*, Chapter 4, Hemisphere Publishing Corporation, New York, NY, pp. 157-97.

Strahle, W.C., Sigman, R.K. and Meyer, W.L. (1987), "Stagnation turbulent flows", *AIAA Journal*, Vol. 25 No. 8, pp. 1071-7.

Tchavdarov, B.M. (1997), "Two-dimensional vortex dynamics of inviscid-viscous interaction at turbulent gas jet impingement", *International Journal of Heat and Fluid Flow*, Vol. 18, pp. 316-27.

Versteeg, H.K. and Malalasekera, W. (1995), "An introduction to computational fluid dynamics, the finite volume method", Longman Scientific and Technical Press, New York, NY.

Erratum

Owing to an error in the production of the article. "Numerical study of turbulent boundary layers with heat transfer and tangential transpiration", pp. 760–82, in *HFF*, Vol. 14 No. 6, the author's name was shown incorrectly.

The author of the article is Burhan Çuhadaroğlu.

Emerald Group Publishing sincerely apologises for this error.